THE ASTROPHYSICAL JOURNAL, 546:1183–1193, 2001 January 10

A SURVEY OF ORGANIC VOLATILE SPECIES IN COMET C/1999 H1 (LEE) USING NIRSPEC AT THE KECK OBSERVATORY

M. J. MUMMA,[1] I. S. MCLEAN,[2] M. A. DISANTI,[1,3] J. E. LARKIN,[2] N. DELLO RUSSO,[1,3] K. MAGEE-SAUER,[4] E. E. BECKLIN,[2] T. BIDA,[5] F. CHAFFEE,[5] A. R. CONRAD,[5] D. F. FIGER,[6] A. M. GILBERT,[7] J. R. GRAHAM,[7] N. A. LEVENSON,[8] R. E. NOVAK,[9] D. C. REUTER,[1] H. I. TEPLITZ,[10] M. K. WILCOX,[2] AND LI-HONG XU[11]

Received 2000 July 5; accepted 2000 August 30

ABSTRACT

The organic volatile composition of the long-period comet C/1999 H1 (Lee) was investigated using the first of a new generation of cross-dispersed cryogenic infrared spectrometers (NIRSPEC, at the Keck Observatory atop Mauna Kea, HI). On 1999 August 19–21 the organics spectral region (2.9–3.7 μm) was completely sampled at both moderate and high dispersion, along with the CO fundamental region (near 4.67 μm), revealing emission from water, carbon monoxide, methanol, methane, ethane, acetylene, and hydrogen cyanide. Many new multiplets from OH in the 1–0 band were seen in prompt emission, and numerous new spectral lines were detected. Several spectral extracts are shown, and global production rates are presented for seven parent volatiles. Carbon monoxide is strongly depleted in comet Lee relative to comets Hyakutake and Hale-Bopp, demonstrating that chemical diversity occurred in the giant-planets' nebular region.

Subject headings: comets: general — comets: individual (Lee (C/1999 H1)) — infrared: solar system — solar system: formation

1. INTRODUCTION

The cometary nucleus contains material that has remained relatively unaltered since the formative phase of the solar system, making comets messengers from this epoch (Mumma, Weissman, & Stern 1993b; Irvine et al. 2000). Do cometary ices faithfully reflect formative conditions in the presolar natal cloud, or did the chemistry of pre-cometary ices vary with distance from the young Sun? The composition and structure of cometary nuclei are key clues to these questions. The long-period and dynamically new comets are thought to have formed in the giant-planets' region of the pre–planetary nebula (5–40 AU) where temperatures ranged from about 200 K near Jupiter to about 40 K near Neptune. Gravitational scattering by the giant planets later ejected them from the inner solar system, forming the Oort cloud—a roughly spherical comet reservoir lying at heliocentric distances beyond 10,000 AU. Stellar perturbations return some Oort cloud comets to the inner solar system, where they then appear as dynamically "new" comets. These can be pumped into long-period orbits by planetary perturbations, and comets Hyakutake, Hale-Bopp, and C/1999 H1 (Lee) belong to this group. A comparison of their compositions can tell us whether conditions in the 5–40 AU nebular zone differed enough to alter the chemistry of their pre-cometary ices.

The composition of native ices (i.e., the fraction stored in the nucleus) tests cometary origins and constrains the types of processing they experienced. Chemical alteration could have resulted from a number of (poorly constrained) processes, such as partial vaporization of icy grain mantles during nebular infall, condensation fractionation of nebular gas, thermal processing of ices, hydrogenation of icy grain mantles, UV photochemistry, and energetic processing by X-rays. Icy grain mantles may have been efficiently hydrogenated in regions of high H-atom density (e.g., an X-ray dissociation region), thereby converting condensed phase CO to CH_3OH and C_2H_2 to C_2H_6. The efficacy of such processing probably varied greatly with heliocentric distance and/or with time, enforcing corresponding differences in the volatile (icy) and refractory organic fractions in comets. However, the compositions of comets Hyakutake and Hale-Bopp were similar to ices in dense interstellar cloud cores, suggesting that little or no alteration occurred in their formative region (Mumma et al. 1996; Mumma 1996, 1997; Crovisier 1999; Bockelée-Morvan et al. 2000).

In this paper, we report the organic volatile composition of the long-period comet Lee. The key organics spectral region (2.9–3.7 μm) was nearly completely sampled at both moderate and high dispersion, and high-dispersion spectra were acquired in the CO fundamental region (near 4.67 μm), using NIRSPEC at the Keck Observatory. These spectra provide the most complete cometary survey at infrared wavelengths to date, and they reveal emission from water, carbon monoxide, methanol, methane, ethane, acetylene, and hydrogen cyanide. Many new multiplets from OH in

[1] Laboratory for Extraterrestrial Physics, Code 690, NASA Goddard Space Flight Center, Greenbelt, MD 20771; mmumma@kuiper.gsfc.nasa.gov.
[2] Department of Physics and Astronomy, University of California, Los Angeles, Los Angeles, CA 90095-1562.
[3] Department of Physics, The Catholic University of America, Washington, DC 20064.
[4] Department of Chemistry and Physics, Rowan University, Glassboro, NJ 08028.
[5] California Association for Research in Astronomy, W. M. Keck Observatory, Kamuela, HI 96743.
[6] Space Telescope Science Institute, 3700 San Martin Drive, Baltimore, MD 21218.
[7] Department of Astronomy, University of California, 601 Campbell Hall, Berkeley, CA 94720-3411.
[8] Department of Physics and Astronomy, Johns Hopkins University, Baltimore, MD 21218.
[9] Department of Physics, Iona College, New Rochelle, NY 10801.
[10] NOAO Research Associate, Laboratory for Astronomy and Solar Physics, Code 681, NASA Goddard Space Flight Center, Greenbelt, MD 20771.
[11] Department of Physical Sciences, University of New Brunswick, Saint John, New Brunswick, E2L 4L5, Canada.

the 1–0 band were seen in prompt emission, and numerous new spectral lines were detected. Several spectral extracts are shown and global production rates are presented for seven parent volatiles. Carbon monoxide is strongly depleted in comet Lee relative to comets Hyakutake and Hale-Bopp, demonstrating that chemical diversity occurred in the giant-planets' nebular region.

2. APPROACH

The study of cometary chemical composition has evolved rapidly in recent years, mainly owing to instrumental advances. At infrared wavelengths, the advent of high dispersion cryogenic spectrometers (e.g., CSHELL, Greene et al. 1993; Tokunaga et al. 1990) opened a new era in cometary science. CSHELL enabled the discovery of symmetric hydrocarbons (methane, ethane, and acetylene) in comet Hyakutake (along with spatially resolved measurements of carbon monoxide and water) (Mumma et al. 1996; Brooke et al. 1996). CSHELL spectra are obtained with high spatial resolution about the nucleus, and this is key to distinguishing gases released directly from nuclear ices (parent volatiles) from those produced or released in the coma (distributed sources) (Dello Russo et al. 1998; DiSanti et al. 1999). However, the CSHELL spectrometer affords a relatively small spectral grasp for each grating setting, so many separate settings are needed to provide adequate spectral coverage for a typical molecular vibrational band. This reduces the efficiency of the approach and limits the prospects for measuring temporal changes in cometary gas production as the nucleus rotates. Such changes are expected if the cometary nucleus is internally heterogeneous.

With larger format detector arrays, higher efficiency is possible without loss of spatial or spectral resolution. The spectrometer can be cross-dispersed so multiple spectral orders can be sampled simultaneously and a larger spectral grasp can be obtained for each order; such instruments are commonly used at optical wavelengths. In 1999, the first such spectrometer for studies at near-infrared wavelengths (1–5.5 μm) became available as a facility instrument on the Keck II 10 m telescope. NIRSPEC is a cross-dispersed echelle spectrograph [1–5.5 μm, resolving power ($\lambda/\delta\lambda$ = RP) $\sim$ 25,000], equipped with a 1024 $\times$ 1024 pixel (Aladdin-2) InSb detector (McLean et al. 1998). Each detector pixel subtends 0.″19 in the spatial direction and 0.″14 in the spectral direction. A flat mirror is mounted back-to-back with the echelle grating, allowing moderate resolution (RP $\sim$ 2000) spectra to be taken (the spatial and spectral directions are exchanged in the moderate resolution mode). A slit-viewing camera (SCAM, featuring a 256 $\times$ 256 pixel (PICNIC) HgCdTe detector array sensitive from 1 to 2.5 μm) provides simultaneous slit viewing and guiding when acquiring spectra in the 1–4.2 μm region. SCAM has a plate scale of 0.″18 pixel^{-1}. A cryogenic image rotator is used to orient the field relative to the fixed slits and to maintain that orientation as the telescope moves. With only three grating settings, NIRSPEC permits a nearly complete high-dispersion survey of the spectral region 2.9–3.7 μm, key for investigating the organic composition of comets.

Comet Lee was discovered in 1999 February, while still approaching the Sun (Lee 1999). Subsequent observations revealed its period to be $\sim$21,000 yr and orbital predictions suggested it would become a favorable target for observations during May–September. We observed comet Lee in 1999 June and August, at similar heliocentric distances before and after its perihelion passage (UT July 11.1, R = 0.708 AU) (Table 1). Here, we present some key results from our postperihelion observations. On UT August 20, we surveyed the L band (2.9–4.2 μm) at moderate dispersion (RP $\sim$ 2000) and acquired high dispersion spectra in the M band (near 4.7 μm). On UT August 21, deep searches for certain key organic species were performed using two echelle/cross-disperser combinations. The slit was oriented east-west on the sky for all observations reported in this paper.

At each grating setting, cometary spectra were acquired using sequences of four scans with a total integration time of 4 minutes on-source per sequence. In the high-dispersion mode, the slit length was 24″ ($\sim$125 detector rows) on the sky, and the telescope was nodded 12″, keeping the comet on-slit for each integration. The comet was switched between the A and B beams in a sequence of either ABAB or ABBA (all data presented here were acquired with ABBA sequencing). During L-band observations, guiding was accomplished using SCAM with the KL filter. However, SCAM cannot be used for guiding while M-band spectra are being acquired, so offset guiding was used during acquisition of CO and H_2O spectra. For each grating setting, spectra of infrared standard stars were acquired for absolute

Table 1

Observing Log Comet Lee[a]

UT Date (1999)	R (AU)	Δ (AU)	Δ-dot (km s^{-1})	RP[b] ($\lambda/\delta\lambda$)	Setting	Targets	On-Source Time (minutes)
June 02.22–02.26.....	1.042	1.099	35.19	25,000	KL_A2	High-Res survey[c]	
June 03.22–03.25.....	1.029	1.12	35.26	25,000	KL_B1	High-Res survey[c]	4
					KL_B2	High-Res survey[c]	4
Aug 19.60–19.66	1.045	1.38	−28.35	25,000	KL_A	High-Res survey[c]	8
				25,000	KL_B	High-Res survey[c]	8
				25,000	KL_C	High-Res survey[c]	8
Aug 20.61–20.66	1.062	1.36	−28.70	2,000	2.9–4.3 μm	Low-Res Survey	4
				25,000	4.7 μm	CO, H_2O	14
Aug 21.59–21.66	1.076	1.35	−29.03	25,000	KL1	C_2H_6, CH_3 OH, CH_4.	24
				25,000	KL2	CH_4, C_2H_2, HCN, 3.425 μm	

[a] R is the heliocentric distance, Δ is the geocentric distance, Δ-dot is the geocentric velocity, and RP is the resolving power ($\lambda/\delta\lambda$).

[b] All high-dispersion spectra (R $\sim$ 25,000) were acquired with the 3 pixel wide slit (0.″43 $\times$ 24″ on the sky). The L-band survey (R $\sim$ 2000) on UT August 20.6 was acquired with the 0.″38 $\times$ 42″ slit.

[c] The high-dispersion survey settings were staggered to cover nearly the entire organics wavelength region 2.9–3.7 μm.

flux calibration of the comet spectra. Stellar spectra were acquired with the same slit width used for the comet, and also with a wider slit to test slit losses. These losses were estimated by assuming an azimuthally symmetric stellar profile, and appropriate corrections were incorporated into the absolute flux calibrations.

Initial data processing included removal of high dark current pixels and cosmic ray hits, and registration of spectral frames. Background emissions from the sky and telescope are removed by subtracting A and B frames. The difference frame reveals cometary emissions as tilted horizontal signatures, positive (*white*) and negative (*black*), respectively (e.g., Figs. 1*a* and 2*a*). The tilted vertical features (*white and black*) are incompletely canceled emission lines from the sky. (NIRSPEC features a quasi-Littrow design to ensure highest optical efficiency. This design introduces some tilt in both spectral and spatial directions, and the anamorphic reimaging optics introduce some additional distortion.) We resampled the frames, straightening the A and B beam within each order independently such that the spectral dimension falls along a row and the spatial dimension is orthogonal to this. Once straightened, residual atmospheric lines were subtracted column-by-column, leaving the cometary signal alone (Figs. 1*b* and 2*b*). Spectra were then extracted from signals present at the A and B beam positions (Figs. 1*c* and 2*c*), and a modeled dust continuum convolved with the synthesized atmospheric transmittance was calculated (Figs. 1*c* and 2*c*). Cometary molecular emissions were isolated by subtracting the modeled dust continuum from the measured spectrum (Figs. 1*d* and 1*e*). Atmospheric transmittance models were calculated using the Spectrum Synthesis Program (SSP) (Kunde & Maguire 1974), which accesses the HITRAN-1992 molecular database (Rothman et al. 1992). SSP models were used to assign wavelength scales to the spectra and to establish absolute column burdens for relevant absorbing species in the terrestrial atmosphere. The transmittance model was binned to the instrumental sampling interval, convolved to the resolution of the comet spectrum, and normalized to the cometary continuum. For additional details on our data processing techniques see Dello Russo et al. (1998) and DiSanti et al. (1999). The extracted comet spectra reveal numerous emission lines from gaseous species (e.g., Fig. 2*c*).

A production rate can be determined for a given species if we first relate the measured line intensities to a column density via an excitation model and then relate the derived column density to an azimuthally averaged (global) production rate. The first step requires a quantum-mechanical model for line-by-line frequencies and strengths within a given rovibrational band; branching ratios and solar fluorescence efficiencies (*g*-factors) can then be developed for individual lines within that band. Their application to intensities measured for individual lines may reveal whether a single temperature characterizes the rotational distribution (the measured intensities are first corrected for atmospheric transmittance at the Doppler-shifted position of each cometary line). If so, the integrated band emission intensity may be obtained from the measured line intensities using *g*-factors appropriate to the derived rotational temperature.

Rotational temperatures for CO and HCN were determined from Boltzmann analyses of individual line intensities (Fig. 5) and were consistent with 75 K (Table 2), as were relative intensities of C_2H_6 *Q*-branches. Rotational temperatures should differ for individual species if radiative cooling controls rotational populations. The similarity of the temperatures retrieved for CO, HCN, and C_2H_6 may reflect the control of rotational populations by electron collisions in the inner coma (Xie & Mumma 1992; see also discussion in Bockelée-Morvan et al. 1994 and Biver et al. 1999). We adopted 75 K as a rotational temperature for species (H_2O, CH_3OH, etc.) for which an independent rota-

Table 2

PARENT VOLATILES IN COMET C/1999 H1 (LEE)

SPECIES[a]	LINE FLUX[b] (10^{-18} W m^{-2}) F1	F2	g_1[b] (10^5 photons s^{-1} molec^{-1})	TEMPERATURE[c] (K)	PRODUCTION RATE (10^{27} s^{-1})	RELATIVE ABUNDANCE
H_2O	3.47	4.77	0.198	(75)	126 ± 10	100.
CO	1.82	3.19	6.84	75 ± 9	2.3 ± 0.2	1.8 ± 0.2
CH_3OH (echelle)	1.00	0.929	1.31	(75)	2.6 ± 0.5	2.1 ± 0.5
CH_3OH (survey)	0.832	1.08	1.31	(75)	2.7 ± 0.5	2.1 ± 0.5
CH_4	1.36	1.47	4.90	(75)	1.02 ± 0.05	0.81 ± 0.08
C_2H_6	4.15	3.91	16.4			
On nucleus				$80\ +25/-19$		
Off nucleus				$65\ +19/-16$	0.84 ± 0.05	0.67 ± 0.07
C_2H_2	0.47	0.46	4.64	(75)	0.34 ± 0.03	0.27 ± 0.03
HCN	2.15	2.39	24.6	72 ± 8	0.29 ± 0.02	0.23 ± 0.02
OH (3046 cm^{-1})[d]	0.48	0.71	0.020			

[a] Observations of H_2O, CO, and CH_3OH (survey) were conducted on UT August 20.6. All other species were observed on UT 1999 August 21.6.

[b] Fluxes are summed over all lines analyzed for each species and are given for two ranges along the slit. For the echelle mode, which includes all entries except the CH_3OH (survey) entry, F1 is the sum included in an aperture 0.″58 × 0.″43 (3 spatial times 3 spectral pixels) in size and centered on the nucleus. For the moderate dispersion mode (CH_3OH survey entry), F1 is the sum included in an aperture 0.″43 by 0.″38 (3 spatial by 2 spectral pixels) in size and centered on the nucleus. For both echelle and moderate dispersion modes, F2 is the total line flux summed over the range 0.″29–2.″0 off the nucleus, averaged east and west. *g*-factors (g_1 is evaluated at $R = 1$ AU) are summed over all lines analyzed as well. The lines used were H_2O (ν_3–ν_2 (0_{00}–1_{01}, 1_{11}–1_{10}), ν_1–ν_2 (1_{01}–2_{12}, 2_{12}–3_{03})), CO (P2 R2 R3 R4), CH_3OH (ν_3 *Q* branch), CH_4 (R0 R1), C_2H_6 ($^RQ_0$ $^RQ_1$ $^RQ_4$ $^PQ_1$ $^PQ_3$ $^PQ_4$), C_2H_2 (R3 P3 P5), HCN (R1 R2 R3 R5 R6 P2 P3 P4 P6 P7 P8), and OH (1–0 P11.5 2^+ and 2^-, P12.5 1^+ and 1^-).

[c] This is the rotational temperature, determined from individual line intensities. When too few lines were available for independent rotational analyses, a representative value (75 K) was adopted (see text).

[d] This is the sum of fluxes measured for the OH quadruplet near 3046 cm^{-1}, consisting of emission from $v' = 1$, $J' = 10.5$ 2^- and 2^+, and $J' = 11.5$ 1^- and 1^+. See Fig. 3*b*. The tabulated *g*-factor assumes that a prompt emission mechanism (see text).

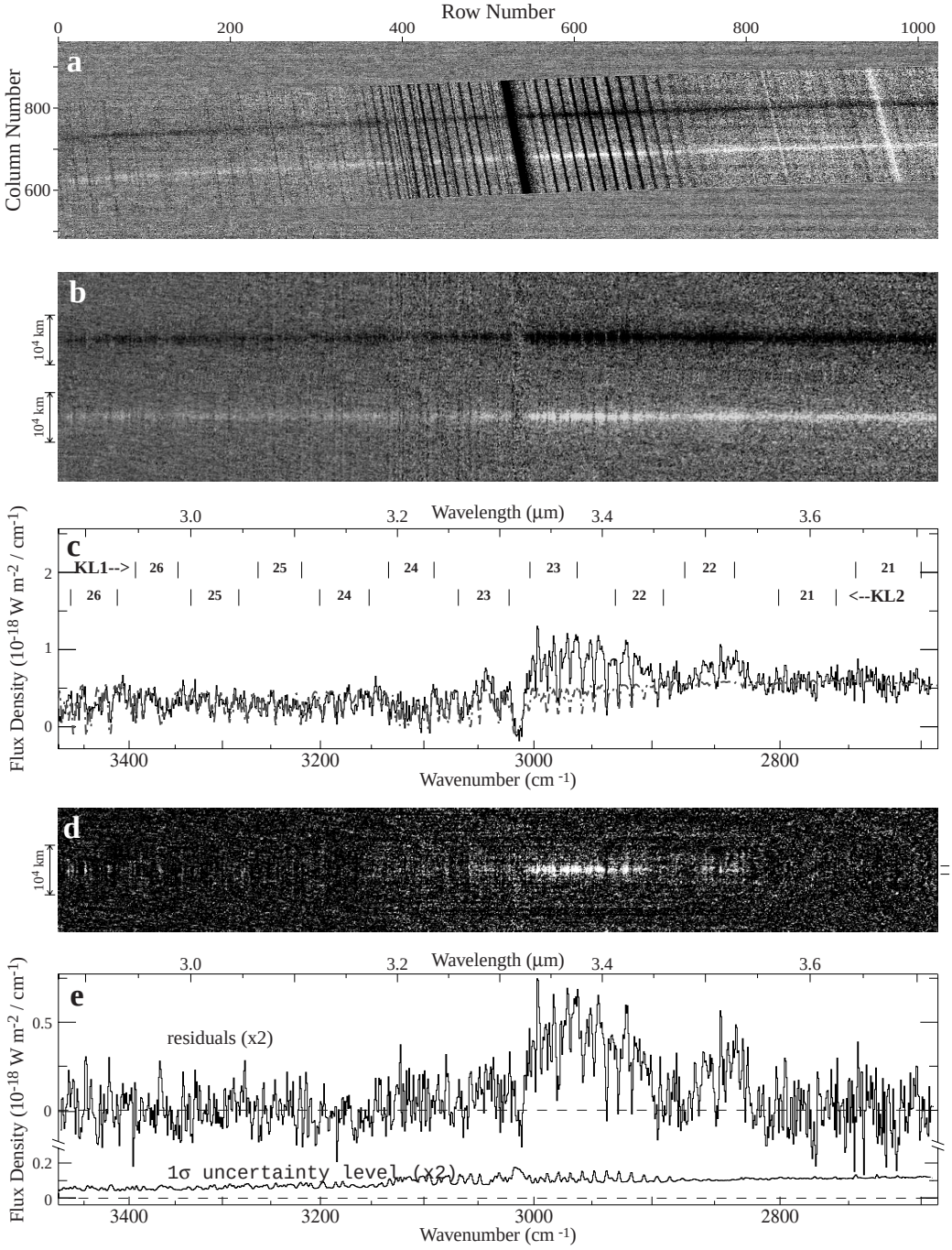

FIG. 1.—Survey spectrum of comet Lee taken in the moderate dispersion mode (RP ~ 2000) on UT 1999 August 20.6. (*a*) The appearance of the spatial-spectral frame (A–B) prior to processing. Of a total of 1024 columns, only the 500 centered on the comet spectrum are shown. Cometary emission appears as two tilted horizontal streaks (white is the A beam, black is the B beam, see text). Residual sky emission appears as many dark and bright diagonal lines (extended across the order from top to bottom). (*b*) The spatial-spectral difference frame after pixel resampling and subtraction of residual sky emission. Cometary continuum and molecular emission features are apparent. (*c*) Moderate resolution spectrum of comet Lee (*solid line*) formed by combining extracts of five rows about each position (A, B). The flux density indicated refers to signal contained within a 0.″38 × 0.″72 aperture centered on the peak continuum emission. A synthetic spectrum of the atmospheric transmittance is also shown (*dashed line*). The extent of individual orders sampled in the echelle mode (RP ~ 25,000) is indicated for the two echelle/cross-disperser settings (KL1 and KL2) used on UT August 21.6. (*d*) Appearance of the difference frame after spatial registration of A and B beams and row-by-row subtraction of the cometary continuum, revealing molecular emissions. Note the extension of emission lines in the spatial direction. (*e*) The spectrum of molecular emissions detected in the survey mode (expanded vertically by a factor of 2). The broad feature centered at 3.52 μm is due to CH_3OH (ν_3) and clearly shows emission from the *P*-, *Q*-, and *R*-branches first seen in comet Austin (1990 V) (Hoban et al. 1991). The broad feature appearing from 3.3–3.45 μm is emission (mainly) from methane, ethane, methanol, and hydroxyl (see text). The channel-by-channel noise amplitude (1 σ) is also shown.

tional temperature could not be determined directly. For certain bands, the intensity may be summed over an entire branch (e.g., the CH_3OH ν_3 *Q*-branch near 3.52 μm); the branching ratio is then used to obtain the emission intensity of the entire band. The extracted production rate is then relatively insensitive to the assumed rotational temperature. At this point, integrated column densities are extracted using the appropriate fluorescence model (Table 2).

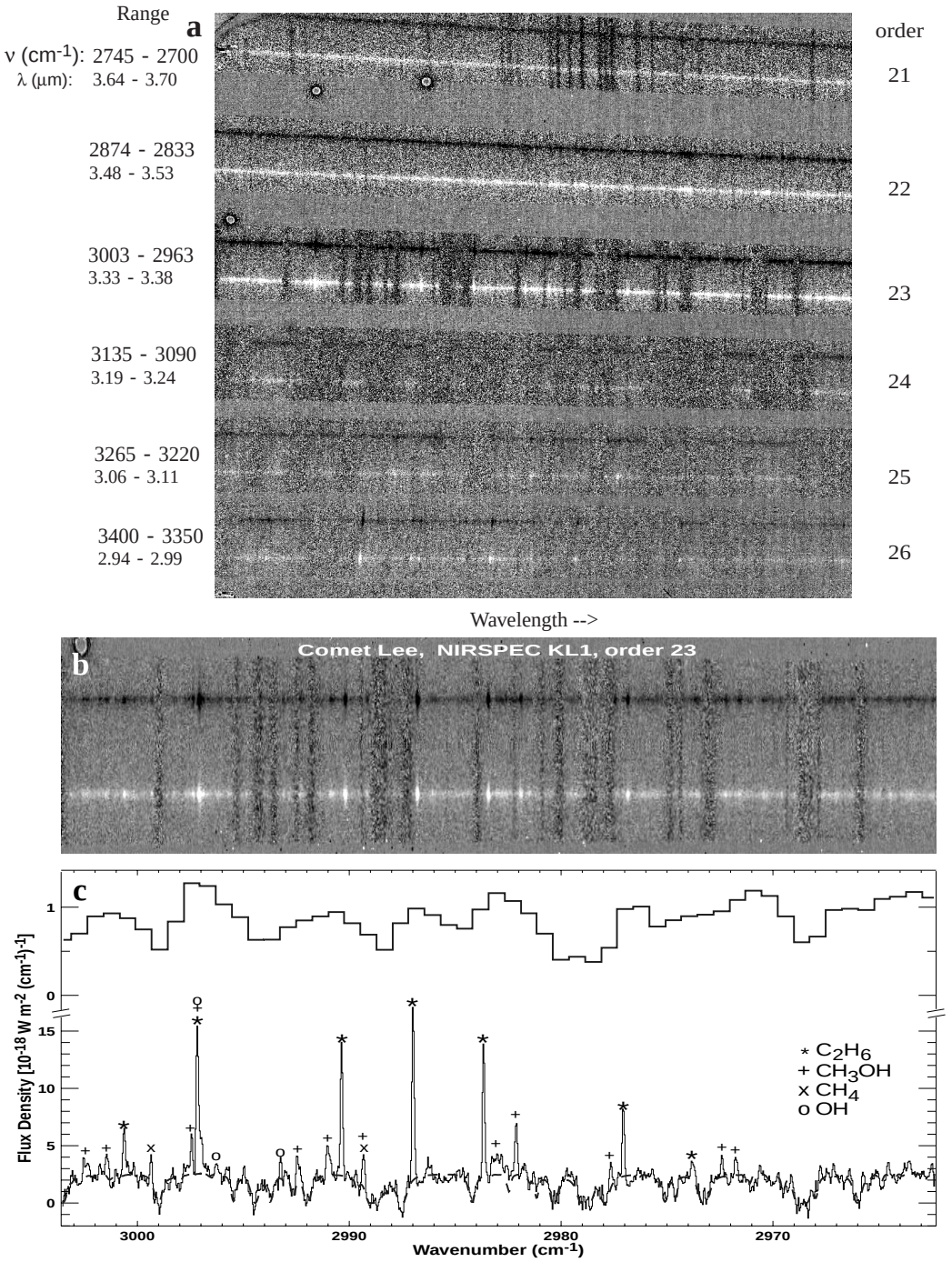

FIG. 2.—High-dispersion spectra (RP ~ 25,000) of comet Lee acquired on UT 1999 August 21.6 using the echelle/cross-disperser setting KL1. Each echelle-grating/cross-disperser setting encompasses multiple orders (6 for the *L* band, 3 for the *M* band) allowing an almost complete survey of the entire organics region (2.85–3.71 μm) with only three grating settings. (*a*) The appearance of the spatial-spectral difference frame (A–B) prior to processing. Cometary continuum and molecular emissions are apparent. (*b*) The spatial-spectral difference of order 23 after registration and sky-subtraction. The speckled features extending entirely across the order (*top to bottom*) are regions of greater stochastic noise, owing to atmospheric emission lines. (*c*) The spectrum (*solid line*) extracted by summing five rows about each beam position. The flux density refers to signal contained within an aperture 0.″43 × 0.″97 centered on the peak continuum emission. A synthetic spectrum of the atmospheric transmittance is also shown (*dashed line*). The marked lines are identified as follows (reading from higher wavenumber to lower): (*) C_2H_6 ν_7 $^RQ_4$ $^RQ_3$ $^RQ_1$ $^RQ_0$ $^PQ_1$ $^PQ_3$ $^PQ_4$; (×) CH_4 ν_3 P2 P3; (+) CH_3OH ν_2 and ν_9 ; (o) OH (1–0) (P12.5 2^+ and 2^-, P13.5 1^+ and 1^-). The moderate resolution spectrum (*histogram*) is shown for comparison.

An apparent production rate (Q) is extracted from the column density by applying a dynamical model featuring spherically symmetric outflow at a uniform velocity (0.8 km s^{-1} in the present case). The trend of these "spherical" production rates versus distance from the nucleus (along the slit) constitutes a Q curve. A "symmetric" Q is constructed by taking the mean of values measured at symmetric distances along slit (east and west) with respect to the nucleus. The nucleus-centered extract is invariably low due to slit losses (primarily caused by seeing), but off-nucleus extracts of the symmetric Q are less affected and they quickly reach a terminal value (unless a distributed source is also present,

DiSanti et al. 1999). This terminal value is taken to be the "global" production rate (see Magee-Sauer et al. 1999a; Dello Russo et al. 1998, 2000 for further discussion).

Global production rates extracted from high-resolution L-band spectra (HCN, C_2H_2, CH_4, C_2H_6, CH_3OH, and OH) were about twofold larger than those obtained from nucleus-centered extracts. On UT August 20, the measured increase was slightly larger—about a factor of 3 for CO and H_2O (from high-dispersion M-band spectra, Fig. 4*a*) and about the same for CH_3OH (from the L-band moderate resolution spectrum, Fig. 1). We attribute this difference to guiding and/or placement of the comet in the slit. The M-band observations used off-axis guiding (which was less effective than SCAM guiding), while a narrower slit was used for the survey spectrum. The production rates given in Table 2 all represent global values, and these are relatively insensitive to guiding and centering of the comet in the slit.

3. RESULTS

Only selected spectra are presented here. We show first the moderate resolution survey spectrum taken on UT August 20 (Fig. 1). The extracted spectrum of molecular emission appears in Fig. 1*e* (note that it is not corrected for atmospheric transmittance). Three main features are seen: the methanol ν_3 vibrational band (centered at 3.52 μm), a feature spanning the 3.3–3.45 μm region (formed mainly by combined emission from bands of methanol ν_2 and ν_9, methane ν_3, and ethane ν_7, but with possible contributions from other organic species and grains), and several isolated spectral emissions near 2.9 μm. The detection of individual spectral lines is suppressed at this relatively low spectral resolving power (RP $\sim$ 2000). Each resolution element is about 1.5 cm^{-1} wide (the dispersion is $\sim$0.77 cm^{-1} pixel^{-1}, and the slit used was 2 pixels wide). The channel-by-channel 1 σ noise level is shown as the bottom trace in Figure 1*e*. The noise level is set by the background flux collected over each resolution element so detection is suppressed if only a single molecular line falls within a resolution element. The detection of individual spectral lines is greatly enhanced at the higher resolving power of the echelle/cross-disperser mode (RP $\sim$ 25,000), and the specific molecular emissions mentioned above are identified in those higher dispersion spectra (see discussion below, and Fig. 2*c*). The spectral coverage of echelle orders sampled with two different echelle/cross-disperser combinations is shown in Figure 1*c*.

A deep search for molecular emission was carried out in the high dispersion mode on UT August 21 (Table 1). We chose our first key echelle/cross-disperser setting (KL1) such that order 23 was centered on the ethane ν_7 band while order 22 sampled the methanol ν_3 band (Fig. 1*c*). Figure 2*a* shows the difference of the raw A and B frames. Six spectral orders are seen, and cometary continuum and spectral emission lines are apparent. Figure 2*b* shows the appearance of order 23 after cleaning, registration, and subtraction of residual sky emission lines—multiple Q-branches of ethane and other cometary emission lines are seen clearly above the brightness level of the continuum. The molecular emissions are extended along the slit. (The continuum is comparably extended but this is masked by the intensity stretch used in Fig. 2*b*.) A spectrum was extracted by summing five rows about the center of each beam, and it is compared with the modeled continuum emission from cometary dust (as extinguished by the terrestrial atmosphere) in Figure 2*c*. Emission lines of ethane (C_2H_6, ν_7), methane (CH_4, ν_3), methanol (CH_3OH, ν_2 and ν_9), and hydroxyl (OH, $v = 1$–0) are marked. Seven Q-branches of ethane ν_7 were detected. Their relative intensities imply a rotational temperature consistent with that derived for HCN and CO ($\sim$75 K, see below). We used 75 K when retrieving the production rate of ethane in comet Lee (Table 2).

The analysis of methanol emission depends on the availability of quantum band models that can be tailored to the low rotational temperatures typical of comets (30–100 K, see discussion in Mumma et al. 2000). These models exist for the ν_3 vibrational band centered near 2844 cm^{-1} but they are only now being developed for ν_2 and ν_9 (Hunt et al. 1991; Reuter 1992; Xu et al. 1997). For this reason, we targeted the ν_3 band in order 22 when selecting the setting KL1. The moderate dispersion spectrum (Fig. 1*e*) reveals a shape for the ν_3 band typical of A-type bands, with a well developed P-, Q-, and R-branch structure; this structure was first resolved in comet Austin 1990 V (Hoban et al. 1991). Those measurements provided the first detection of cometary methanol, which was confirmed several weeks later by independent millimeter observations of a methanol rotational line (Bockelée-Morvan et al. 1991). Similar structure in the infrared was later seen in other comets, for example 109P/Swift-Tuttle (Davies et al. 1993; DiSanti et al. 1995). The underlying band structure is seen more clearly in high dispersion spectra of comet Lee, revealing a prominent triply peaked Q-branch and a dense grouping of individual P- and R-branch lines (Fig. 3*a*). A similar triply peaked Q-branch structure was seen in CSHELL spectra of comets C/1996 B2 (Hyakutake) and C/1995 O1 (Hale-Bopp) (M. J. Mumma et al. 2000, private communication). We were unable to determine a rotational temperature from the observed methanol lines, so we adopted a value typical of other measured species (75 K). We tailored the quantum band model of Xu et al. to 75 K and used it to obtain a g-factor for the Q-branch region (we used the rest frequency range 2843.2–2846.8 cm^{-1}). Production rates derived from high- and moderate- dispersion spectra are in agreement (Table 2).

Our second key echelle/cross-disperser setting (KL2) was optimized for detection of HCN and acetylene in order 25, and methane in order 23 (Fig. 1*c*). Although long expected and sought in comets, methane was first detected in comet Hyakutake (Mumma et al. 1996), and later in comet Hale-Bopp (Weaver et al. 1999; Mumma et al. 1997). The strongest emission lines of the ν_3 band (R0, R1) were expected to appear in order 23 of setting KL2 (Fig. 3*b*), along with the weaker lines (P2, P3) detected in order 23 of setting KL1 (Fig. 2*b*). We adopted a rotational temperature of 75 K when deriving a production rate for methane. The relative abundance of methane in comet Lee (Table 2) is similar to that found for Hyakutake and Hale-Bopp (Mumma et al. 1996; Weaver et al. 1999).

A new quadruplet of lines was serendipitously detected in order 23, near 3046 cm^{-1} (Fig. 3*b*); they are emitted by vibrationally excited OH in high rotational states ($v' = 1$, $J' = 10.5, 11.5$). Such high-J lines cannot be excited by fluorescent pumping (either ultraviolet or infrared) of thermalized OH in the coma. Moreover, their intensities are peaked on the nucleus of comet Lee, and their spatial profiles mimic those observed for parent volatiles and dust. These are the properties expected for "prompt" emission (Mumma 1982; Weaver & Mumma 1984; Crovisier 1989). In prompt emission, dissociative excitation of H_2O creates

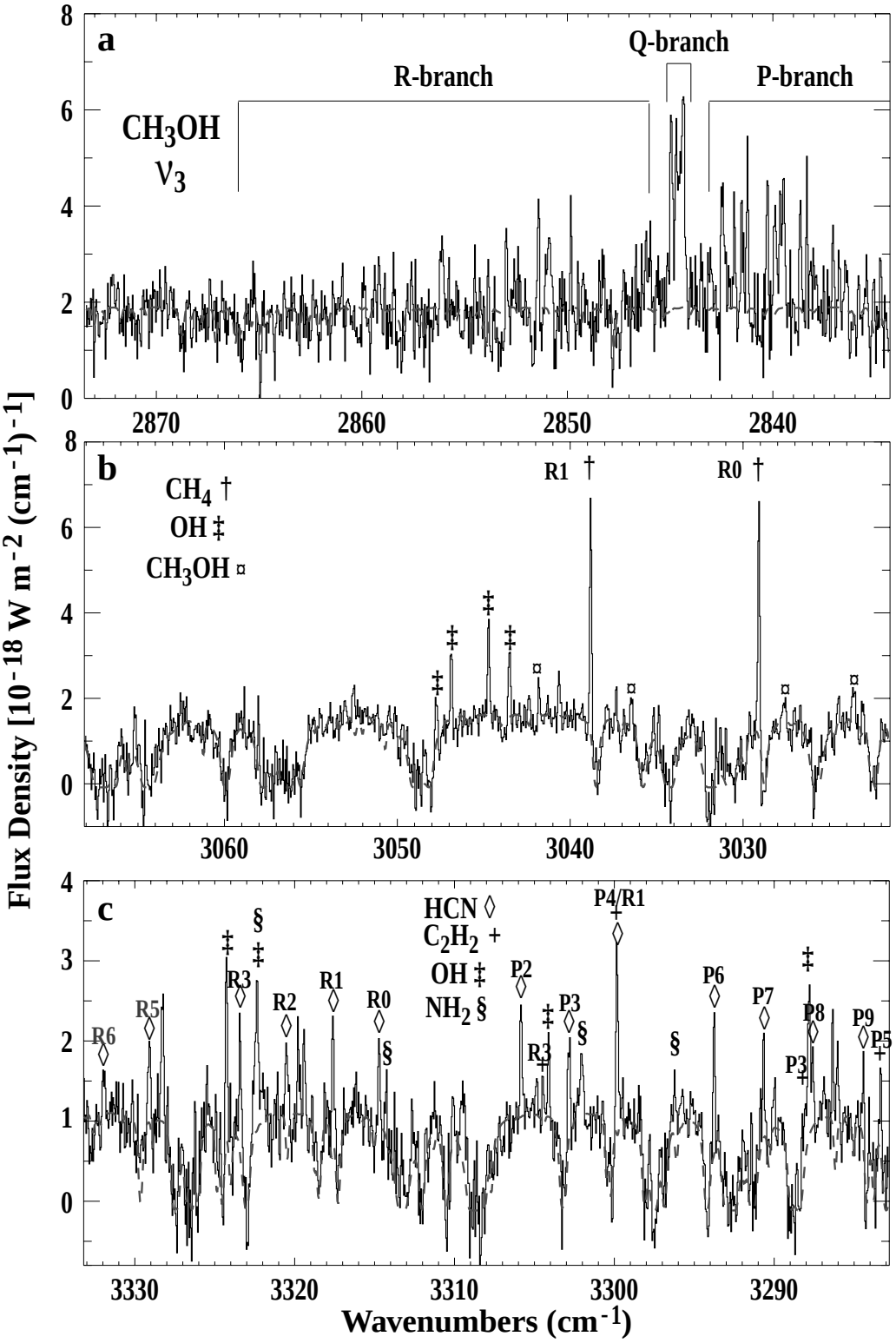

FIG. 3.—Selected high-dispersion spectra of comet Lee, acquired on UT August 21.6. Synthetic atmospheric transmittance spectra are shown for comparison (*dashed lines*). (*a*) KL filter, setting 1, order 22: CH_3OH ν_3. The triply peaked *Q*-branch is prominent and many lines in the *P*- and *R*-branches are also detected. (*b*) KL filter, setting 2, order 23: OH (1–0) (P11.5 2^+ and 2^-, P12.5 1^+ and 1^-); and CH_4 ν_3 R1 and R0. The cometary methane lines are seen Doppler-shifted by ~ -27 km s^{-1} relative to their terrestrial counterparts, owing to the comet's geocentric motion. (*c*) KL filter, setting 2, order 25: Identified lines include HCN ν_3 (13 lines); NH_2 (4 lines) OH (1–0) (P6.5 1^- and 2^+); and C_2H_2 ν_4 R3 and P5. Some of the "unknown" emissions in this order are preliminarily consistent with hot-band lines of H_2O; however, detailed modeling of line positions and intensities is required.

OH fragments in rotationally and vibrationally excited states (Yamashita 1975; Andresen et al. 1984). The newly formed OH promptly radiates a vibrational quantum (within a few milliseconds), and the rotational distribution then cools to ambient temperatures by collisions, making subsequent fluorescent or collisional excitation of the observed lines negligible. The spatial distribution of "prompt" emission thus traces that of the parent species

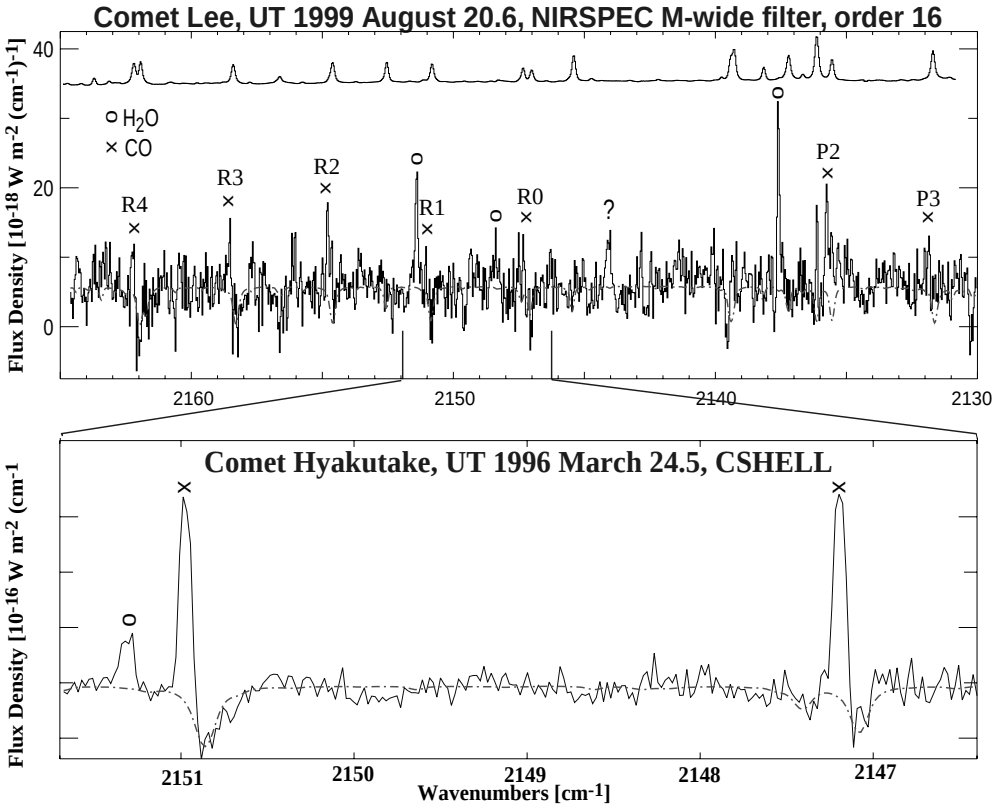

FIG. 4.—CO in comets Lee and Hyakutake. (*Top*) High-dispersion spectrum of comet Lee in the *M* band near 4.7 μm, acquired on UT August 20.6. Spectral lines of the CO $v = 1$–0 fundamental band (7 lines) and H_2O-band emissions are seen. Also shown are the modeled transmittance (*dashed line*) and the observed sky emission spectrum (*top*, *solid line*). The cometary lines are blueshifted by ~ -27 km s^{-1} ($\sim +0.21$ cm^{-1}) relative to their rest frequencies. CO line assignments are indicated. The three water lines are identified as follows (cf. Dello Russo et al. 2000), from left to right: 001–010 (ν_3–ν_2) band, rotational designation 1_{11}–1_{10} (rest frequency 2151.19 cm^{-1}); 100–010 (ν_1–ν_2) band, rotational designation 0_{00}–1_{11} (rest frequency 2148.19 cm^{-1}); ν_3–ν_2 band, rotational designation 0_{00}–1_{01} (rest frequency 2137.37 cm^{-1}). An unidentified emission appears near 2144 cm^{-1}. (*bottom*) CSHELL spectrum of comet Hyakutake taken on UT 1996 March 24.5 in this same spectral region. This figure reveals the vastly different chemical composition (i.e., CO-to-water ratio) of these two comets (see text for details). The increased spectral grasp attainable with NIRSPEC is evident (only one of three simultaneously obtained NIRSPEC echelle *M*-band orders is shown).

(water) and not the flatter distribution exhibited by fluorescent emission from general OH in the coma. Prompt and fluorescent OH emission was reported near 3.0 μm for Hyakutake (Brooke et al. 1996; Magee-Sauer et al. 1999b) and Hale-Bopp (Magee-Sauer et al. 1999a), but these emissions were not analyzed quantitatively. Four OH emission lines were detected near 3.04 μm in comet Hyakutake (Brooke et al. 1996), two from $v' = 1$ ($J' = 5.5$) and two from $v' = 2$ ($J' = 2.5$). Brooke et al. noted that the spatial distribution of lines from $v' = 1$ were peaked on the nucleus as expected for prompt emission excited from a water parent, but lines from $v' = 2$ were more extended as expected if ultraviolet fluorescence of OH were responsible.

The excitation efficiency (*g*-factor) for OH prompt emission is determined by the solar ultraviolet flux responsible for dissociative excitation (mainly Lyα) and by the quantum structure of the water molecule (Crovisier 1989). We compared the infrared flux measured for the four OH lines near 3046 cm^{-1} with the production rate measured for H_2O, and we derived an effective *g*-factor for this combined multiplet (Table 2). This *g*-factor may be used to derive water production rates in other comets. OH multiplets were also detected in several other high-dispersion spectra (e.g., Figs. 2*c*, 3*c*, and other echelle orders not shown), but their analysis is deferred to a later publication.

Order 25 (KL2 setting) is dominated by the ν_3 vibrational band of HCN, but it also contains lines of C_2H_2, NH_2, both prompt and fluorescent emission from OH, and strong lines that are preliminarily consistent with the $2\nu_1$–ν_1 band of H_2O (Fig. 3*c*). Thirteen lines of HCN were detected, permitting an accurate determination of its rotational temperature (72 ± 8 K) and production rate (Fig. 5, Table 2). The 11 lines used in the rotational analysis stem from excited levels ($J' = 1$–7) which together contain $\sim$80% of the entire population in the 001 vibrational level; their combined intensities represent $\sim$65% of the integrated ν_3 vibrational band emission. Three lines of the ν_3 band of acetylene (R3, P3, and P5) were also detected in this order. The band *g*-factor for C_2H_2 is nearly a factor of 2 smaller than that of HCN, hence for similar column densities the integrated intensity for the acetylene ν_3 band is only about half as bright as the HCN ν_3 band. Moreover, even-*J* lines of acetylene are even less favorable for detection because nuclear spin statistics make them weaker than odd-*J* lines by a factor of 3. Odd-*J* lines of C_2H_2 should be more favorable for detection, but many are coincidentally in regions of poor atmospheric transmittance. These combined effects cause the number of C_2H_2 lines detected to be small compared with HCN.

Eight lines of the CO ($v = 1$–0) 4.7 μm fundamental band fall within order 16 in the *M* band, and seven of them were detected (Fig. 4*a*). Of these, four were sufficiently strong to extract reliable spatial profiles, and these were used in our analysis. They span upper state levels with rotational

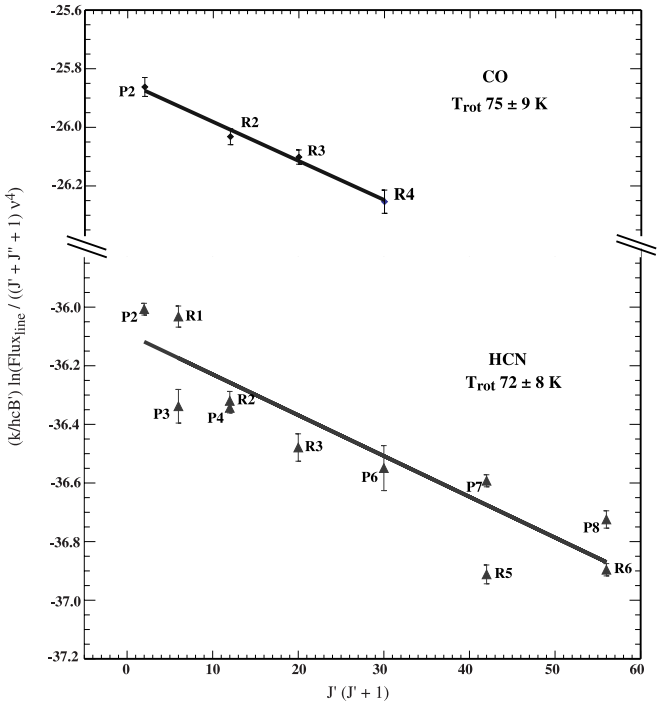

FIG. 5.—Boltzmann analyses of rotational temperatures for CO (4 lines, observed on UT August 20.6) and HCN (11 lines, observed on UT August 21.6). CO line intensities were extracted for a 2.″90 × 0.″43 box centered on the comet nucleus, and the retrieved rotational temperature was 75 ± 9 K. HCN intensities were extracted for a 0.″58 × 0.″43 box centered on the comet nucleus, and the retrieved rotational temperature was 72 ± 8 K.

quantum number $J' = 1$ through 5, sufficient to provide a good rotational temperature via a standard Boltzmann analysis (Fig. 5, Table 2). For a rotational temperature of 75 K, these four lines represent 27% of the integrated 1–0 vibrational band intensity, and the populations they sample (in levels $J' = 1, 3, 4, 5$) represent ~53% of the entire population in $v' = 1$. Retrieval of production rates followed the procedure described by DiSanti et al. (1999).

We see no evidence for a distributed source of CO emission in comet Lee. The Q-curve derived for CO in comet Lee reaches a terminal value within 1″ (~1000 km) of the nucleus, consistent with release from a purely native source. For comet Lee, the telescope was nodded 12″ along slit, hence the net signal (A − B/B + A) from a spatially extended emission should cancel increasingly as the midpoint is approached (an east-west symmetric profile will exactly cancel midway between the beams). If sufficiently strong, the CO signal (sum of nuclear and distributed sources) should be detected near each end of the slit in the difference frame, but we see no net signal there above the noise. In comet Hale-Bopp at 1.06 AU, the terminal Q was reached only beyond 5000 km from the nucleus, after the distributed source was fully developed (DiSanti et al. 1999). While we cannot completely eliminate the possibility of a distributed source for CO in comet Lee, it is evidently much less abundant than in comet Hale-Bopp in which the native and distributed fractions each produced about one-half of the total CO.

Two water hot-band lines also appear in this order, and two more lines appear in order 15 (not shown). These lines were first detected in comets Hyakutake and Hale-Bopp, along with lines of another water hot-band near 2 μm (Dello Russo et al. 2000; Mumma et al. 1996). They are excited by nonresonance fluorescence and provide a direct method for measuring water production in comets (Mumma et al. 1995; Bockelée-Morvan et al. 1989). An independent rotational temperature could not be derived from the measured water lines because they vary similarly with temperature. We adopted a temperature (75 K) representative of other species when deriving a production rate for water (Table 2).

4. DISCUSSION

We measured global production rates for seven parent volatile species in comet Lee (Table 2). We see no evidence of a distributed source for any species, so we take these production rates to represent the abundances of native (nuclear) ices. Their relative abundances are similar to those found for comets Hyakutake and Hale-Bopp (two other comets from the giant-planets' nebular region), excepting CO, which is deficient in comet Lee by a factor of 5–10.

Cometary C_2H_2 and C_2H_6were first detected in Hyakutake (Brooke et al. 1996; Mumma et al. 1996), and Mumma et al. (1996) argued that their abundances were consistent with conversion of condensed phase C_2H_2 to C_2H_6 by H-atom addition to pre-cometary ices. Their relative abundances in Hale-Bopp were similar in those in Hyakutake (Weaver et al. 1999; Dello Russo et al. 1999; Magee-Sauer et al. 1999c), and they were consistent with predictions of gas-grain models for dense cloud cores (Hasegawa, Herbst, & Leung 1992; Hasegawa & Herbst 1993a, 1993b). We compare our production rates for comet Lee (Table 2) with those obtained for Hyakutake and Hale-Bopp using common data extraction procedures (Dello Russo et al 1999; Magee-Sauer et al. 1999c), except the production rate for acetylene in Hyakutake which is taken from Brooke et al. (1996). The ethane abundances (Lee, Hyakutake, Hale-Bopp) are (0.67% ± 0.07%, 0.64% ± 0.15%, and 0.56% ± 0.04%) and acetylene abundances are (0.27% ± 0.03%, 0.3%/0.9%, and 0.31% ± 0.1%). Ethane and acetylene are found with similar abundance in these three comets, supporting a common initial C_2H_2 endowment and similar H-atom processing.

Ethylene (C_2H_4) is an intermediate product of H-atom addition but interstellar models predict a much lower abundance for it compared with ethane and acetylene. Laboratory measurements of H-atom addition to acetylene ice at 10 K demonstrate that abundant ethane is produced but ethylene is not found, probably because conversion of ethylene to ethane is much faster than its production from acetylene (Hiraoka et al. 1999, 2000). A much lower abundance of C_2H_4 compared with C_2H_2 and C_2H_6 would be consistent with these laboratory results. Ethylene was searched for but was not found in Hyakutake and Hale-Bopp (M. J. Mumma et al. 2000, private communication) and in comet Lee (this work). However, the attainment of meaningful upper limits must await development of a fluorescence model for ethylene. Detections of C_2H_2, C_2H_4, and C_2H_6 in comet Halley were reported from neutral mass spectrometric measurements (Eberhardt 1999; preliminary abundances were ~0.3%, ~0.3%, and ~0.4%, respectively). However, C_2H_4 appears at the same mass peak as N_2 and CO, the latter of which has much higher abundance in comet Halley. The reported detection must be regarded with caution pending presentation of a full analysis.

The abundance of native CO in comet Lee (1.8% ± 0.2%) is much lower than in comets Halley (3.5%, Eberhardt

1999), Hyakutake (5.8%, Mumma et al. 1996), and Hale-Bopp (12.3% ± 0.7%, DiSanti et al. 1999). (The value reported in Mumma et al. 1996 was based on an extract taken on the nucleus, and likely suffers from optical depth effects. The true native CO abundance in Hyakutake is probably greater than the reported value.) However, the methanol abundance is similar in these four comets: Lee (2.1% ± 0.5%), Halley (1.7% ± 0.04%, Eberhardt et al. 1994), Hyakutake (1.7%, Biver et al. 1999), and Hale-Bopp (~2%, Despois 1999). CO can be converted to formaldehyde and methanol by H-atom addition to CO ice at 10–20 K (Hiraoka et al. 1994, 1998), and Mumma et al. (1996) suggested that such processing had influenced the $CO:H_2CO:CH_3OH$ chemistry of ices in comet Hyakutake.

The much lower CO/CH_3OH ratio (~1) for comet Lee suggests that the initial CO endowment and/or the conversion efficiency differed, compared with the other comets. The dwell time of H-atoms on grain surfaces varies strongly with temperature, and when coupled with different rate constants could lead to a strong dependence of conversion efficiency with temperature and with species (e.g., CO vs. C_2H_2). We have seen that the abundances of symmetric hydrocarbons in these comets are in good agreement, together suggesting the importance of H-atom addition reactions in the formation of abundant ethane. However, the methanol and CO abundances in these comets do not reveal any trends, suggesting that H-atom addition to CO in pre-cometary ice is not the primary mechanism for forming CH_3OH in these comets or that other factors (such as formation temperature) are involved.

Could CO have been preferentially lost from comet Lee by thermal processing of the nucleus after accretion? Methane, acetylene, and ethane are apolar species, and CO has a relatively small dipole moment ($\mu = 0.11$ D; Lang 1980). Thus, their ices are hypervolatile compared with (hydrogen-bonded) ices of polar species (e.g., water, methanol, and hydrogen cyanide, for which $\mu = 1.85$, 1.70, and 2.98 D, respectively). Thermal processing should cause depletions of hypervolatiles by factors related to their surface bonding strengths, with methane showing depletions similar to CO but acetylene and ethane only slightly less so. This is not observed; the abundances of ethane, methane, and acetylene are similar in the four comets [the upper limit for methane in comet Halley (<1%; Eberhardt 1999) is consistent with abundances detected in the other three comets], hence we infer that CO was not preferentially lost by this mechanism. Comets from the giant-planets' region exhibit a wide range in methanol abundance, ~0.5%/5% relative to water (Mumma 1997; Mumma et al. 1993a; Bockelée-Morvan, Brooke, & Crovisier 1995), and CO is also known to vary strongly among them, perhaps suggesting that formation temperature is an important factor. If so, the abundance ratios may lead ultimately to a temperature probe for the formative region. The strong depletion of CO in the presence of "normal methanol" and a "normal" ratio of acetylene to ethane suggest that comet Lee received a reduced initial abundance of CO ice compared with Hyakutake and Hale-Bopp. Comet Halley may be intermediate. This difference is consistent with chemical diversity for ices in the pre-planetary disk at distances of 5–40 au from the young Sun.

Our detection of prompt emission from OH quadruplets near 3046 cm^{-1} and other frequencies is significant for two reasons. First, OH prompt emission could contribute to several unidentified features seen in cometary spectra. The four lines near 3046 cm^{-1} would appear at a mean wavelength of 3.285 μm when measured at moderate resolution, and they could contribute to the excess emission found near that wavelength in comet Swift-Tuttle (3.28–3.29 μm, Davies et al. 1993), and previously assigned to an unidentified organic species. Our moderate resolution spectrum of comet Lee shows an enhancement in this spectral region, encompassing combined emission from the OH multiplet and from methane R1 (cf., Figs. 1*c*, 1*e*, and 3*b*). OH prompt emission could also contribute (along with water hot bands) to the unidentified 2.8 μm emission feature discovered in comet 1P/Halley (Tokunaga, Nagata, & Smith 1989; Crovisier 1989; Bockelée-Morvan & Crovisier 1989).

Second, OH prompt emission may provide a convenient and temperature-insensitive method for measuring water production in future comets. A similar process leads to dissociative excitation of $O(^1D)$, and the ensuing 630 nm prompt emission has been used to infer water production rates in many comets (Spinrad et al. 1982; Magee-Sauer et al. 1988; Fink & Hicks 1996; Combi et al. 1999). The excitation of prompt emission is determined by the solar ultraviolet flux responsible for dissociative excitation (mainly Lyα) and by the quantum structure of the water molecule. For this reason, the excitation efficiency is not highly sensitive to the rotational temperature of the water molecule. The prompt emitter can sometimes be produced from more than one cometary species, e.g., water is the dominant source of $O(^1D)$ but small amounts are also produced by dissociative excitation of other parent volatiles (e.g., CO, CO_2) and of free-radical species (e.g., OH, Magee-Sauer et al. 1988). The high rotational state of the OH prompt emission observed here is diagnostic of production by water, but a small contribution from other parent volatiles might be possible and must be evaluated. Based on their intensities and on the expected relative insensitivity of prompt emission to details of the rotational distribution of water, we expect OH prompt emission to provide an important additional method for determining water production rates in comets.

The advent of the NIRSPEC instrument has introduced a truly remarkable new capability to cometary science. The ability to detect and compare seven parent volatiles in only a few hours, without incurring the uncertainties resulting from temporal variability or the systematic errors introduced by using disparate detection systems and telescopes, is critical to the task of determining cometary composition. A wealth of information about the physical state of a comet's atmosphere is also gained through the measurement of rotational temperatures, production rates, and spatial profiles. The application of NIRSPEC and similar cross-dispersed infrared array-based spectrometers to future comets will provide a more complete taxonomy for these bodies and thus will lead to a better understanding of physical and chemical conditions in the early solar system.

This work was supported by the NASA Planetary Astronomy Program under RTOP 344-32-30-07 to M. J. M. and grant NAG5-7905 to M. A. D., by the NASA Planetary Atmospheres Program under grant NAG5-7753 to N. D. R., and by the National Science Foundation under grant AST-9619461 to K. M.-S. L.-H. X. acknowledges support from the Natural Sciences and Engineering Research Council of Canada. Data presented herein were

obtained at the W. M. Keck Observatory, which is operated as a scientific partnership among the California Institute of Technology, the University of California and the National Aeronautics and Space Administration. The Observatory was made possible by the generous financial support of the W. M. Keck Foundation. It is a pleasure to acknowledge the hard work and dedication of the NIRSPEC instrument team at UCLA: Maryanne Anglionto, Odvar Bendiksen, George Brims, Leah Buchholz, John Canfield, Kim Chim, Jonah Hare, Fred Lacayanga, Samuel B. Larson, Tim Liu, Nick Magnone, Gunnar Skulason, Michael Spencer, Jason Weiss, and Woon Wong. In addition, we thank the observing assistants at Keck observatory: Joel Aycock, Gary Puniwai, Charles Sorenson, Ron Quick, and Wayne Wack.

REFERENCES

Andresen, P., Ondrey, G. S., Titze, B., & Rothe, E. W. 1984, J. Chem. Phys., 80, 2548
Biver, N., et al. 1999, AJ, 118, 1850
Bockelée-Morvan, D., Brooke, T. Y., & Crovisier, J. 1995, Icarus, 116, 18
Bockelée-Morvan, D., Colom, P., Crovisier, J., Despois, D., & Paubert, G. 1991, Nature, 350, 318
Bockelée-Morvan, D., & Crovisier, J. 1989, A&A, 216, 278
Bockelée-Morvan, D., et al. 2000, A&A, 353, 1101
Bockelée-Morvan, D., Padman, R., Davies, J. K., & Crovisier, J. 1994, Planet. Space Sci., 42 (8), 665
Brooke, T. Y., Tokunaga, A. T., Weaver, H. A., Crovisier, J., Bockelée-Morvan, D., & Crisp, D. 1996, Nature, 383, 606
Combi, M. R., Cochran, A. L., Cochran, W. D., Lambert, D. L., & Johns-Krull, C. M. 1999, ApJ, 512, 961
Crovisier, J. 1989, A&A, 213, 459
———. 1999, Earth Moon Planets, 79(1), 125
Davies, J. K., Mumma, M. J., Reuter, D. C., Hoban, S., Weaver, H. A., Puxley, P. J., & Lumsden, S. L. 1993, MNRAS, 265, 1022
Dello Russo, N., DiSanti, M. A., Mumma, M. J., Magee-Sauer, K., & Rettig, T. W. 1998, Icarus, 135, 377
Dello Russo, N., Mumma, M. J., DiSanti, M. A., Magee-Sauer, K., Novak, R., & Rettig, T. W. 1999, BAAS, 31(4), 1098
———. 2000, Icarus, 143, 324
Despois, D. 1999, Earth Moon Planets, 79(1), 103
DiSanti, M. A., Mumma, M. J., Dello Russo, N., Magee-Sauer, K., Novak, R., & Rettig, T. W. 1999, Nature, 399, 662
DiSanti, M. A., Mumma, M. J., Geballe, T. R., & Davies, J. K. 1995, Icarus, 116, 1
Eberhardt, P. 1999, Space Sci. Rev., 90, 45
Eberhardt, P., Meier, R., Krankowsky, D., & Hodges, R. R. 1994, A&A, 288, 315
Fink, U., & Hicks, M. D. 1996, ApJ, 459, 729
Greene, T. P., Tokunaga, A. T., Toomey, D. W., & Carr, J. S. 1993, Proc. SPIE, 1946, 311
Hasegawa, T. I., & Herbst, E. 1993a, MNRAS, 261, 83
———. 1993b, MNRAS, 263, 589
Hasegawa, T. I., Herbst, E., & Leung, C. M. 1992, ApJS, 82, 167
Hiraoka, K., Miyagoshi, T., Takayama, T., Yamamoto, K., & Kihara, Y. 1998, ApJ, 498, 710
Hiraoka, K., Ohashi, N., Kihara, Y., Yamamoto, K., Sato, T., & Yamashita, A. 1994, Chem. Phys. Lett., 229, 408
Hiraoka, K., Takayama, T., Euchi, A., Handa, H., & Sato, T. 2000, ApJ, 532, 1029
Hiraoka, K., Yamamoto, K., Kihara, Y., Takayama, T., & Sato, T. 1999, ApJ, 514, 524
Hoban, S., Mumma, M. J., Reuter, D. C., DiSanti, M., Joyce, R. R., & Storrs, A. 1991, Icarus, 93, 122
Hunt, R. H., Shelton, W. N., Cook, W. B., Bignall, O. N., Mirick, J. W., & Flaherty, F. A. 1991, J. Mol. Spectrosc., 149, 252
Irvine, W., F. Schloerb, P., Crovisier, J., Fegley, B., & Mumma, M. J. 2000, in Protostars and Planets IV, ed. V. Mannings, A. P. Boss, & S. S. Russell (Tucson: Univ. Arizona Press), 1159
Kunde, V. G., & Maguire, W. C. 1974, J. Quant. Spectrosc. Radiat. Transf., 14, 803
Lang, K. R. 1980, Astrophysical Formulae (Berlin: Springer), 162
Lee, S. 1999, IAU Circ. 7144
Magee-Sauer, K., Mumma, M. J., DiSanti, M. A., Dello Russo, N., & Rettig, T. W. 1999a, Icarus, 142, 498
———. 1999b, Asteroids, Comets, Meteors Conf. (Ithaca: Cornell Univ. Press)
Magee-Sauer, K., Mumma, M. J., DiSanti, M. A., & Dello Russo, N. 1999c, BAAS, 31(4), 1123
Magee-Sauer, K., Roesler, F. L., Scherb, F., Harlander, J., & Oliversen, R. J. 1988, Icarus, 76, 89
McLean, I. S., et al. 1998, Proc. SPIE, 3354, 566
McLean, I. S., et al. 2000, PASP, submitted
Mumma, M. J. 1982, in Vibrational Rotational Spectroscopy for Planetary Atmospheres (NASA CP-2223), 717
———. 1996, Nature, 383, 581
———. 1997, in ASP Conf. Ser. 122, From Stardust to Planetesimals: Review Papers, ed. Y. Pendleton & A. G. G. M. Tielens (San Francisco: ASP), 369
Mumma, M. J., DiSanti, M. A., Dello Russo, N., Fomenkova, M., Magee-Sauer, K., Kaminski, C. D., & Xie, D. X. 1996, Science, 272, 1310
Mumma, M. J., DiSanti, M. A., Dello Russo, N., Magee-Sauer, K., Novak, R., & Fomenkova, M. 1997, IAU Circ. 6573
Mumma, M. J., DiSanti, M. A., Dello Russo, N., Magee-Sauer, K., & Rettig, T. W. 2000, ApJ, 531, L155
Mumma, M. J., DiSanti, M. A., Tokunaga, A. T., & Roettger, E. E. 1995, BAAS, 27, 1144
Mumma, M. J., Hoban, S., Reuter, D. C., & DiSanti, M. 1993a, in IAU Symp. 160, Asteroids, Comets, and Meteors (Houston: Lunar Planet. Inst.), 227
Mumma, M. J., Weissman, P. R., & Stern, S. A. 1993b, in Protostars and Planets III, ed. E. H. Levy & J. I. Lunine (Tucson: Univ. Ariz. Press), 1177
Reuter, D. C. 1992, ApJ, 386, 330
Rothman, L. S., et al. 1992, J. Quant. Spectrosc. Radiat. Transf., 48, 469
Spinrad, H. 1982, PASP, 94, 1008
Tokunaga, A. T., Nagata, T., & Smith, R. G. 1989, A&A, 187, 519
Tokunaga, A. T., Toomey, D. W., Carr, J., Hall, D. N. B., & Epps, H. W. 1990, Proc. SPIE, 1235(2), 131
Weaver, H. A., & Mumma, M. J. 1984, ApJ, 285, 872
Weaver, H. A., Brooke, T. Y., Chin, G., Kim, S. J., Bockelée-Morvan, D., & Davies, J. K. 1999, Earth Moon Planets, 78, 71
Xie, X., & Mumma, M. J. 1992, ApJ, 386, 720
Xu, Li-Hong, Wang, X., Cronin, T. J., Perry, D. S., Fraser, G. T., & Pine, A. S. 1997, J. Mol. Spectrosc., 185, 158
Yamashita, I. 1975, J. Phys. Soc. Japan, 39, 205